IEEE Open Journal of Signal Processing

Received 25 October 2022; revised 20 January 2023; accepted 27 January 2023. Date of publication 13 February 2023; date of current version 23 February 2023. The review of this article was arranged by Associate Editor Fan Liu.

Digital Object Identifier 10.1109/OJSP.2023.3244427

Robust Tensor Decomposition for Heterogeneous Beamforming Under Imperfect Channel State Information

KENGO ANDO [1] (Graduate Student Member, IEEE), KOJI ISHIBASHI [2] (Senior Member, IEEE), AND GIUSEPPE THADEU FREITAS DE ABREU [1] (Senior Member, IEEE)

[1]School of Computer Science and Engineering, Constructor University, 28759 Bremen, Germany
[2]Advanced Wireless and Communication Research Center, University of Electro-Communications, Chofu, Tokyo 182-8585, Japan

CORRESPONDING AUTHOR: KENGO ANDO (e-mail: kando@constructor.university).

ABSTRACT We propose a new robust variation of the tensor decomposition known as the multi-linear generalized singular value decomposition (ML-GSVD), and demonstrate its effectiveness in the design of joint transmit (TX) and receive (RX) beamforming (BF) for both the downlink (DL) and the uplink (UL) of cell-free massive multiple-input multiple-output (CF-mMIMO) systems. The new technique, dubbed the robust orthogonality-enforcing ML-GSVD (ROEML-GSVD), mitigates the degradation in the DL and UL BF design due to the tensor decomposition error and the channel state information (CSI) imperfection by exploiting their independence. Numerical results demonstrate that the proposed method is highly effective, leading not only to a significant reduction on the tensor decomposition error compared to state-of-the-art (SotA) methods, but also to the improvement in the data rate achieved by the subsequent beamformers in heterogeneous scenarios where users have distinct numbers of antennas.

INDEX TERMS Heterogeneous cell-free massive MIMO systems, tensor decomposition, transmit and receive beamforming.

I. INTRODUCTION

A key enabling technology for beyond fifth generation (5G+) and sixth generation (6G) wireless communications is CF-mMIMO systems [1], [2], [3], [4], [5], [6], [7]. In order to suppress multi-user interference (MUI) from massive numbers of active user equipment (UE), CF-mMIMO systems realize efficient BF utilizing a large number of spatially distributed access points (APs), which transmit collaboratively under the control of a central processing unit (CPU).

To be truly useful, however, CF-mMIMO systems must be able to handle users with arbitrary and distinct numbers of antennas [8], [9]. To that end, a joint TX and RX BF scheme for user-heterogeneous CF-mMIMO systems based on a tensor decomposition dubbed the orthogonality-enforcing multilinear generalized singular value decomposition (OEML-GSVD) was proposed in [5]. In that design, the instantaneous channel tensor was decomposed by the proposed OEML-GSVD, enabling the available orthogonalized subspaces to be exclusively allocated to each UE. Thanks to this feature, the spectral efficiency (SE) performance of CF-mMIMO systems can be significantly improved by OEML-GSVD-based BF, compared to previous SotA alternatives [1], [2], [3], [10], so long as perfect CSI is available.

However, in CF-mMIMO systems, the extraordinarily large channel dimensions [11] often impose the reutilization and length limitation of pilot sequences, both of which are sources of non-orthogonality among pilot sequences and, consequently, of CSI imperfection [12]. Moreover, since BF optimization based on singular value decomposition (SVD)-like methods strongly relies on knowledge of instantaneous channel structure, practically achievable SE can be significantly degraded in the presence of CSI imperfection [13]. Indeed, also the OEML-GSVD-based BF design of [5] is heavily affected by CSI imperfection because it is fundamentally a generalization of the SVD-BF of [14], from the earlier point-to-point multiple-input multiple-output (MIMO) setting to more recent heterogeneous multi-user CF-mMIMO setting. It follows from the latter that improving the robustness against

CSI imperfection is crucial for practical effectiveness of BF design in CF-mMIMO systems.

In turn, tensor decomposition algorithms such as OEML-GSVD and the earlier multilinear generalized singular value decomposition (ML-GSVD) [15], [16] have inherent decomposition errors even if perfect CSI is available, such that accuracy of the tensor-based BF approach is exposed to both sources of degradation. This article aims to mitigate this issue, by adding to the OEML-GSVD-based BF design method of [5] robustness to both CSI imperfection and to the tensor decomposition error, yielding a new robust OEML-GSVD (ROEML-GSVD) scheme and corresponding TX and RX BF for both DL and UL transmissions. The main contributions of this article can be summarized as follows:

- We present a new CSI imperfection-aware robust tensor decomposition algorithm, named ROEML-GSVD, which is capable of simultaneously decomposing multiple channel matrices of different sizes in a structured manner with a common right-multiplying component, that significant simplifies the joint TX and RX beamformers for user-heterogeneous CF-mMIMO systems;
- Building on the above, a new BF design scheme is proposed, which in addition to incorporating the aforementioned CSI error awareness decomposition, is also robust to the decomposition errors themselves, and consequently substantially outperform SotA alternatives.

Notation: Real-valued column vectors and matrices are denoted in bold face and capitalized bold face letters, respectively, while their complex-valued counterparts are represented in corresponding italic boldface, respectively. Tensors are represented by bold capital letters in calligraphic font (*e.g.*$\boldsymbol{\mathcal{X}}$), and their n-th mode unfolding is denoted by $\boldsymbol{\mathcal{X}}_{(n)}$. The n-th power of a matrix $\boldsymbol{X}$ is denoted as $\boldsymbol{X}^n$. The ℓ_1, ℓ_2 and Frobenius norms are denoted by $\|\cdot\|_1$, $\|\cdot\|_2$ and $\|\cdot\|_{\mathrm{F}}$, respectively. The element-wise absolute value, transpose, conjugate transpose, inverse, trace, vectorize, diagonalize and block diagonalize operations are represented as $|\cdot|$, $(\cdot)^{\mathrm{T}}$, $(\cdot)^{\mathrm{H}}$, $(\cdot)^{-1}$, Tr[·], vec(·), diag(·), blkdiag(·), respectively. The imaginary unit, the $N\times N$ identity matrix, the $N\times 1$ all-1 column vector, and the Khatri-Rao product are respectively denoted by j, $\mathbf{I}_N$, $\mathbf{1}_N$, and $\diamond$. The k-th column of the matrix $\boldsymbol{X}$ is denoted as $\langle \boldsymbol{X}\rangle_k$. The complex Gaussian distributions with mean ν_n and variance σ_n^2 is denoted by $\mathcal{CN}(\nu_n, \sigma_n^2)$.

II. SYSTEM MODEL

Consider a CF-mMIMO system as illustrated in Fig. 1, composed of L APs placed over the lattice points of a uniform square grid, covering a squared service area of sides D [m] long, each equipped with N antennas and connected through wired unbounded fronthaul links to a single CPU, serving both the UL and DL transmissions of K uniformly and randomly distributed heterogeneous UEs, with each k-th UE equipped with M_k of antennas. For future convenience, the indices of all APs and UEs will be collected in the sets $\mathcal{L} \triangleq \{1, \ldots, L\}$ and $\mathcal{K} \triangleq \{1, \ldots, K\}$, respectively.

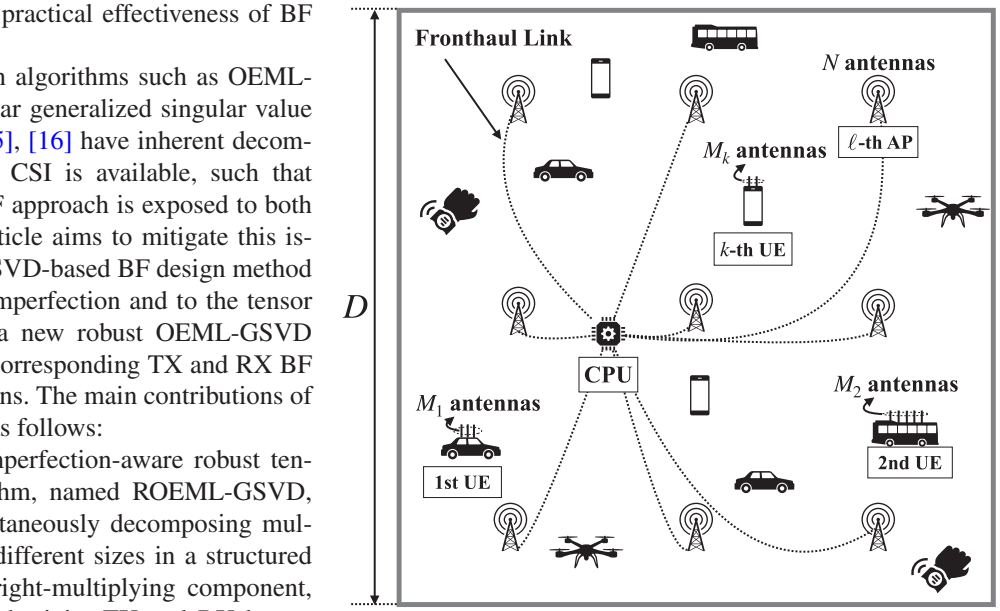

FIGURE 1. User-heterogeneous CF-mMIMO system.

Following preceding work on CF-mMIMO [1], [2], [3], [4], [5] and relying on channel reciprocity, it is assumed that the network operates in time division duplex (TDD) fashion, with UL training phase and subsequent DL and UL data communication phases. It is furthermore assumed, however, that the CSI acquired during the UL training phase is subject to channel estimation errors, with the CSI imperfection modeled as additive noise [17], [18]. Then, the true and imperfectly estimated spatially correlated fading channels between the ℓ-th AP and the k-th UE, respectively denoted $\boldsymbol{H}_{\ell,k}$ and $\hat{\boldsymbol{H}}_{\ell,k}$, are modeled as [19], [20]

$$\boldsymbol{H}_{\ell,k} \triangleq \rho_{\ell,k}\boldsymbol{R}_{\ell,k}^{1/2}\boldsymbol{G}_{\ell,k}\left(\boldsymbol{T}_{\ell,k}^{1/2}\right)^{\mathrm{T}} \in \mathbb{C}^{M_k\times N}, \tag{1}$$

$$\hat{\boldsymbol{H}}_{\ell,k} \triangleq \sqrt{1-\gamma^2}\boldsymbol{H}_{\ell,k} + \gamma\rho_{\ell,k}\tilde{\boldsymbol{G}}_{\ell,k} \in \mathbb{C}^{M_k\times N} \tag{2}$$

where the matrices $\boldsymbol{T}_{\ell,k} \triangleq \boldsymbol{a}(\theta_{\ell,k})\boldsymbol{a}(\theta_{\ell,k})^{\mathrm{H}} \in \mathbb{C}^{N\times N}$ and $\boldsymbol{R}_{\ell,k} \triangleq \boldsymbol{a}(\vartheta_{\ell,k})\boldsymbol{a}(\vartheta_{\ell,k})^{\mathrm{H}} \in \mathbb{C}^{M_k\times M_k}$ model the spatially correlated scattering at the ℓ-th AP and k-th UE, with $\boldsymbol{a}(\theta_{\ell,k})$ and $\boldsymbol{a}(\vartheta_{\ell,k})$ denoting the array steering vectors of uniform linear array (ULA) antennas with angle of departure (AoD) $\theta_{\ell,k}$ and angle of arrival (AoA) $\vartheta_{\ell,k}$, respectively; the matrices $\boldsymbol{G}_{\ell,k}$ and $\tilde{\boldsymbol{G}}_{\ell,k} \in \mathbb{C}^{M_k\times N}$ carry random and independent additive Gaussian variates [17], [18], such that $\mathrm{vec}(\boldsymbol{G}_{\ell,k})$, $\mathrm{vec}(\tilde{\boldsymbol{G}}_{\ell,k}) \sim \mathcal{CN}(0, \mathbf{I}_{NM_k})$; $\gamma \in [0, 1]$ is a parameter controlling the quality of channel estimation; and $\rho_{\ell,k} = 10^{\frac{-\delta(d_{\ell,k})}{20}}$ denotes the amplitude of the channel characterized by the large-scale fading coefficients $\delta(d_{\ell,k})$, determined by the urban macro cell path loss model [21]

$$\delta(d_{\ell,k}) = 22.7 + 36.7\log_{10}(d_{\ell,k}) + 26\log_{10}(f_{\mathrm{c}}), \tag{3}$$

where f_{c} denotes the carrier frequency and $d_{\ell,k}$ is the distance between the ℓ-th AP and the k-th UE.

For future convenience, we define the concatenated actual channel matrix $\boldsymbol{H}_k \triangleq [\boldsymbol{H}_{1,k}, \ldots, \boldsymbol{H}_{L,k}] \in \mathbb{C}^{M_k \times LN}$, the estimated channel matrix $\hat{\boldsymbol{H}}_k \triangleq [\hat{\boldsymbol{H}}_{1,k}, \ldots, \hat{\boldsymbol{H}}_{L,k}] \in \mathbb{C}^{M_k \times LN}$, and the estimation error matrix $\tilde{\boldsymbol{G}}_k \triangleq [\tilde{\boldsymbol{G}}_{1,k}, \ldots, \tilde{\boldsymbol{G}}_{L,k}] \in \mathbb{C}^{M_k \times LN}$, respectively.

Following the above, in DL mode, the complex baseband received signal $\boldsymbol{y}_k^{\mathrm{d}} \in \mathbb{C}^{Q_k \times 1}$ at the k-th UE subject to the TX-BF matrices $\boldsymbol{V}_k^{\mathrm{d}} \in \mathbb{C}^{LN \times Q_k}$ and RX-BF matrices $\boldsymbol{U}_k^{\mathrm{d}} \in \mathbb{C}^{Q_k \times M_k}$ can be written as

$$\boldsymbol{y}_k^{\mathrm{d}} = \overbrace{\boldsymbol{U}_k^{\mathrm{d}} \boldsymbol{H}_k \boldsymbol{V}_k^{\mathrm{d}} \boldsymbol{s}_k^{\mathrm{d}}}^{\text{Intended signal}} + \overbrace{\sum_{k' \in \mathcal{K} \setminus \{k\}} \boldsymbol{U}_k^{\mathrm{d}} \boldsymbol{H}_k \boldsymbol{V}_{k'}^{\mathrm{d}} \boldsymbol{s}_{k'}^{\mathrm{d}}}^{\text{Downlink inter-user interference}} + \overbrace{\boldsymbol{U}_k^{\mathrm{d}} \boldsymbol{n}_k^{\mathrm{d}}}^{\text{Colored noise}}, \tag{4a}$$

where $\boldsymbol{s}_k^{\mathrm{d}} \in \mathbb{C}^{Q_k \times 1}$ denotes an informative symbol vector of length Q_k while $\boldsymbol{n}_k^{\mathrm{d}} \sim \mathcal{CN}(0, \sigma^2 \mathbf{I}_{M_k})$ describes the additive white Gaussian noise (AWGN) vector at the k-th UE.

In turn, in the UL, the estimated signal $\hat{\boldsymbol{s}}_k^{\mathrm{u}} \in \mathbb{C}^{Q_k \times 1}$ from the k-th UE subject to the TX-BF matrices $\boldsymbol{V}_k^{\mathrm{u}} \in \mathbb{C}^{M_k \times Q_k}$ and RX-BF matrices $\boldsymbol{U}_k^{\mathrm{u}} \in \mathbb{C}^{Q_k \times LN}$ can be written as

$$\hat{\boldsymbol{s}}_k^{\mathrm{u}} = \overbrace{\boldsymbol{U}_k^{\mathrm{u}} \boldsymbol{H}_k^{\mathrm{T}} \boldsymbol{V}_k^{\mathrm{u}} \boldsymbol{s}_k^{\mathrm{u}}}^{\text{Intended signal}} + \overbrace{\sum_{k' \in \mathcal{K} \setminus \{k\}} \boldsymbol{U}_k^{\mathrm{u}} \boldsymbol{H}_{k'}^{\mathrm{T}} \boldsymbol{V}_{k'}^{\mathrm{u}} \boldsymbol{s}_{k'}^{\mathrm{u}}}^{\text{Uplink inter-user interference}} + \overbrace{\boldsymbol{U}_k^{\mathrm{u}} \boldsymbol{n}^{\mathrm{u}}}^{\text{Colored noise}}, \tag{4b}$$

where $\boldsymbol{s}_k^{\mathrm{u}} \in \mathbb{C}^{Q_k \times 1}$ denotes an informative symbol vector of length Q_k while $\boldsymbol{n}^{\mathrm{u}} \sim \mathcal{CN}\left(0, \sigma^2 \mathbf{I}_{LN}\right)$ describes the AWGN vector at all the APs.

It follows from (4), that the DL SE η_k^{d} and the UL SE η_k^{u} corresponding to a given k-th UE, are given by

$$\eta_k^{\mathrm{d}} = \log_2 \left(\det \left(\mathbf{I}_{Q_k} + \boldsymbol{U}_k^{\mathrm{d}} \boldsymbol{H}_k \boldsymbol{F}_k^{\text{TX-d}} \boldsymbol{H}_k^{\mathrm{H}} \boldsymbol{U}_k^{\mathrm{d}\mathrm{H}} \boldsymbol{E}_k^{\mathrm{d}\,-1} \right) \right), \tag{5a}$$

with

$$\boldsymbol{E}_k^{\mathrm{d}} \triangleq \sum_{k' \in \mathcal{K} \setminus \{k\}} \boldsymbol{U}_k^{\mathrm{d}} \boldsymbol{H}_k \boldsymbol{F}_{k'}^{\text{TX-d}} \boldsymbol{H}_k^{\mathrm{H}} \boldsymbol{U}_k^{\mathrm{d}\mathrm{H}} + \sigma_k^2 \boldsymbol{F}_k^{\text{RX-d}}, \tag{5b}$$

and

$$\eta_k^{\mathrm{u}} = \log_2 \left(\det \left(\mathbf{I}_{Q_k} + \boldsymbol{U}_k^{\mathrm{u}} \boldsymbol{H}_k^{\mathrm{T}} \boldsymbol{F}_k^{\text{TX-u}} \boldsymbol{H}_k^{*} \boldsymbol{U}_k^{\mathrm{u}\mathrm{H}} \boldsymbol{E}_k^{\mathrm{u}\,-1} \right) \right), \tag{6a}$$

with

$$\boldsymbol{E}_k^{\mathrm{u}} \triangleq \sum_{k' \in \mathcal{K} \setminus \{k\}} \boldsymbol{U}_k^{\mathrm{u}} \boldsymbol{H}_{k'}^{\mathrm{T}} \boldsymbol{F}_{k'}^{\text{TX-u}} \boldsymbol{H}_{k'}^{*} \boldsymbol{U}_k^{\mathrm{d}\mathrm{H}} + \sigma_k^2 \boldsymbol{F}_k^{\text{RX-u}}, \tag{6b}$$

where we have used $\boldsymbol{F}_k^{\text{TX-d}} \triangleq \boldsymbol{V}_k^{\mathrm{d}} \boldsymbol{V}_k^{\mathrm{d}\mathrm{H}}$, $\boldsymbol{F}_k^{\text{RX-d}} \triangleq \boldsymbol{U}_k^{\mathrm{d}} \boldsymbol{U}_k^{\mathrm{d}\mathrm{H}}$, $\boldsymbol{F}_k^{\text{TX-u}} \triangleq \boldsymbol{V}_k^{\mathrm{u}} \boldsymbol{V}_k^{\mathrm{u}\mathrm{H}}$, and $\boldsymbol{F}_k^{\text{RX-u}} \triangleq \boldsymbol{U}_k^{\mathrm{u}} \boldsymbol{U}_k^{\mathrm{u}\mathrm{H}}$.

III. ROBUST TENSOR DECOMPOSITION FOR HETEROGENEOUS CHANNEL ESTIMATES WITH CSI-IMPERFECTION

A. THE ROEML-GSVD DESIGN

Thanks to the ML-GSVD [15], [16], each slice $\boldsymbol{H}_k$ of the tensor $\boldsymbol{\mathcal{H}}$ can be split into the private matrices $\boldsymbol{B}_k$ and $\mathbf{C}_k$, and the common matrix $\boldsymbol{A}$, as described by (see also Fig. 2)

$$\boldsymbol{H}_k = \boldsymbol{B}_k \mathbf{C}_k \boldsymbol{A}^{\mathrm{T}} + \boldsymbol{W}_k \tag{7}$$

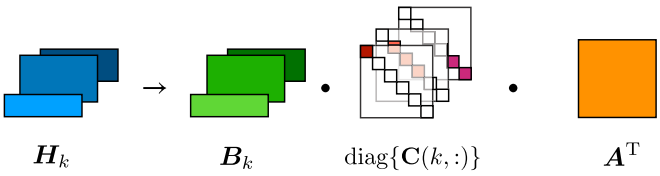

FIGURE 2. Illustration of the proposed ROEML-GSVD.

where $\boldsymbol{B}_k \in \mathbb{C}^{M_k \times LN}$ is a unitary matrix with $\boldsymbol{B}_k \boldsymbol{B}_k^{\mathrm{H}} = \mathbf{I}_{M_k}$, $\boldsymbol{A} \in \mathbb{C}^{LN \times LN}$ is a square matrix, and $\mathbf{C} \in [0, 1]^{K \times LN}$ is a rectangular matrix, such that the k-th row of $\mathbf{C}$ is used to construct the diagonal matrix $\mathbf{C}_k = \mathrm{diag}\left(\langle \mathbf{C}^{\mathrm{T}} \rangle_k\right)$.

In view of (7), and in presence of CSI imperfection, the CSI available for the i-th iteration of the tensor decomposition algorithm at the k-th user can be written as[1]

$$\hat{\boldsymbol{H}}_k = \sqrt{1 - \gamma^2} \left(\boldsymbol{B}_k^{(i)} \boldsymbol{\Gamma}_k^{(i)} + \boldsymbol{W}_k^{(i)} \right) + \gamma \tilde{\boldsymbol{G}}_k \boldsymbol{\Omega}_k, \tag{8}$$

where γ denotes a channel estimation error factor[2], $\boldsymbol{W}_k^{(i)} \in \mathbb{C}^{M_k \times LN}$ denotes a fitting error matrix and we implicitly defined the matrices $\boldsymbol{\Gamma}_k^{(i)} \triangleq \mathbf{C}_k^{(i)} \boldsymbol{A}^{(i)\mathrm{T}}$ and $\boldsymbol{\Omega}_k \triangleq \mathrm{diag}\left([\rho_{1,k} \mathbf{1}_N^{\mathrm{T}}, \ldots, \rho_{L,k} \mathbf{1}_N^{\mathrm{T}}]^{\mathrm{T}}\right)$ for future convenience.

Under the ML-GSVD [15], [16], the matrices $\boldsymbol{A}^{(i)}$, $\boldsymbol{B}_k^{(i)}$ and $\mathbf{C}_k^{(i)}$ are updated iteratively solving the unitary constrained optimization (direct fitting) problem [28]

$$\boldsymbol{B}_k = \underset{\boldsymbol{B}_k}{\mathrm{argmin}} \quad \mathbb{E}\left[\mathrm{Tr}\left(\boldsymbol{W}_k \boldsymbol{W}_k^{\mathrm{H}}\right)\right] \tag{9a}$$

$$\text{subject to } \boldsymbol{B}_k \boldsymbol{B}_k^{\mathrm{H}} = \mathbf{I}_{M_k}, \tag{9b}$$

which can be readily achieved using the Lagrangian $\mathcal{L}_{\mathrm{B}}$,

$$\mathcal{L}_{\mathrm{B}} = \mathbb{E}\left[\mathrm{Tr}\left(\boldsymbol{W}_k \boldsymbol{W}_k^{\mathrm{H}}\right) + \mathrm{Tr}\left(\boldsymbol{L}_{\mathrm{m}} \left(\boldsymbol{B}_k \boldsymbol{B}_k^{\mathrm{H}} - \mathbf{I}_{M_k}\right)\right)\right], \tag{10}$$

where $\boldsymbol{L}_{\mathrm{m}} \in \mathbb{C}^{M_k \times M_k}$ is the Lagrange multiplier matrix.

Due to (8), the CSI error dependent expression of the decomposition error matrices $\boldsymbol{W}_k$ becomes

$$\boldsymbol{W}_k = \frac{\hat{\boldsymbol{H}}_k - \gamma \tilde{\boldsymbol{G}}_k \boldsymbol{\Omega}_k}{\sqrt{1 - \gamma^2}} - \boldsymbol{B}_k \boldsymbol{\Gamma}_k, \tag{11}$$

such that the Wirtinger solution of (9) under imperfect CSI as assumed here yields

$$\boldsymbol{B}_k^{(i+1)} = \hat{\boldsymbol{H}}_k \boldsymbol{\Gamma}_k^{(i)\mathrm{H}} \left(\boldsymbol{\Gamma}_k^{(i)} \left(\hat{\boldsymbol{H}}_k^{\mathrm{H}} \hat{\boldsymbol{H}}_k + \gamma^2 \boldsymbol{\Omega}_k^{\mathrm{H}} \boldsymbol{\Omega}_k \right) \boldsymbol{\Gamma}_k^{(i)\mathrm{H}} \right)^{-\frac{1}{2}}, \tag{12}$$

while $\mathbf{C}^{(i+1)}$ is updated as usual via

$$\mathbf{C}^{(i+1)} = \boldsymbol{\mathcal{D}}_{(3)}^{(i+1)} \left(\boldsymbol{\Psi} \left(\boldsymbol{A}^{(i)} \diamond \mathbf{I}_{LN} \right)^{\mathrm{H}} \right)^{\mathrm{T}}, \tag{13}$$

where $\boldsymbol{\Psi} \triangleq \mathrm{diag}\left\{ \frac{1}{\|\langle \boldsymbol{A}^{(i)} \rangle_1\|_2^2 + \omega}, \ldots, \frac{1}{\|\langle \boldsymbol{A}^{(i)} \rangle_{LN}\|_2^2 + \omega} \right\}$, with the small quantity ω added to avoid infinite ratios; and $\boldsymbol{\mathcal{D}}^{(i+1)}$ denotes

[1] Equation (8) is widely used to model CSI estimates subjected to errors. See [22, Eq.(5)] and [23, Eq.(4)] for examples and [24] for an overview.

[2] Various techniques for the estimation of the parameter γ can be found in related literature, *e.g.* [25], [26], [27]. See also [13] for a concise overview.

Algorithm 1: ROBUST OEML-GSVD.

Choice Parameters: Set ε, δ, ξ, ω, and $i_{\max}$.
Input: $\mathcal{H}=\left[\hat{\boldsymbol{H}}_1,\ldots,\hat{\boldsymbol{H}}_K\right]$ and γ
Output: $\boldsymbol{B}_k$, $\mathbf{C}$, and $\boldsymbol{A}$

Initialize $\boldsymbol{A}$ and $\mathbf{C}$ as in [5];
for $i=0,1,\ldots,i_{\max}$ **do**
  Construct $\boldsymbol{B}_k$ as per (12);
  Update $\mathbf{C}$ using (13), (14), and (15);
  Update $\boldsymbol{A}$ using (16);
end for

the tensor of the matrices $\boldsymbol{D}_k^{(i+1)}\triangleq\boldsymbol{B}_k^{(i+1)\mathrm{H}}\hat{\boldsymbol{H}}_k$, with $\mathcal{D}_{(n)}^{(i+1)}$ denoting its n-th mode unfolding [29].

Since (13) allows for $\mathbf{C}$ to be complex-valued and unbounded, an operation akin to thresholding strategy widely employed in compressing sensing [30] must be applied to box constrain and normalize each ℓ_n-th column $\langle\mathbf{C}^{(i+1)}\rangle_{\ell_n}$ of $\mathbf{C}^{(i+1)}$, yielding [5]

$$\left\langle\mathbf{C}^{(i+1)}\right\rangle_{\ell_n}\leftarrow\frac{\left|\left\langle\mathbf{C}^{(i+1)}\right\rangle_{\ell_n}\right|}{\max\left(\left|\left\langle\mathbf{C}^{(i+1)}\right\rangle_{\ell_n}\right|,\varepsilon\right)},\tag{14}$$

where $\ell_n\in\{1,\ldots,LN\}$, and $0<\varepsilon\ll 1$.

Furthermore, in order to ensure that the resources allocated to different users are orthogonal [5], all but M_k elements of the k-th row of $\mathbf{C}$ are zero-forced, *i.e.*,

$$c_{k,\ell_n}^{(i+1)}\leftarrow 0,\ \forall\,\ell_n\in\mathcal{Z}_k,\tag{15a}$$

where $\mathcal{Z}_k$ is the set of indices of the smallest $LN-M_k$ elements of the k-th row of $\mathbf{C}$.

Next, in order to avoid the underutilization of spatial resources and take full advantage of the degrees of freedom (DoF) of $\mathcal{H}$, the following projection is applied to the non-zero elements $\mathbf{C}$ if and only if $LN\geq\sum_k M_k$: 1) randomly partition the set of free dimensions $\mathcal{F}\triangleq\{\ell_n\big|\|\langle\mathbf{C}\rangle_{\ell_n}\|_1=0,\ \forall\,\ell_n\in\{1,\ldots,LN\}\}$ into K mutually-exclusive subsets $\mathcal{F}_k$, each with cardinality $|\mathcal{F}_k|=M_k-\|\langle\mathbf{C}^{\mathrm{T}}\rangle_k\|_1$ such that $\mathcal{F}_k\cap\mathcal{F}_{k'}=\emptyset$, $(k\neq k')$; then, 2) allocate the subspaces in $\mathcal{F}_k$ to the k-th user by making [5]

$$c_{k,\ell_n}^{(i)}\leftarrow 1,\ \forall\,\ell_n\in\mathcal{F}_k,\ \forall\,k.\tag{15b}$$

Finally, the right-hand side of the matrix $\boldsymbol{A}$ is updated via

$$\boldsymbol{A}^{(i+1)\mathrm{T}}=\mathcal{D}_{(1)}^{(i+1)}\boldsymbol{\Theta}+\xi\mathbf{I}_{LN},\tag{16}$$

with $\boldsymbol{\Theta}\triangleq\mathrm{blkdiag}\left\{\frac{\langle\mathbf{C}\rangle_1^{\mathrm{H}}}{\|\langle\mathbf{C}\rangle_1\|_2^2+\delta},\ldots,\frac{\langle\mathbf{C}\rangle_{LN}^{\mathrm{H}}}{\|\langle\mathbf{C}\rangle_{LN}\|_2^2+\delta}\right\}$, where δ and ξ are sufficiently small quantities inserted to avoid divergent ratios and ensure the full-rankness of $\boldsymbol{A}$, respectively.

The updates given in (12)–(16) are repeatedly computed until the solution converges. The procedure of the proposed ROEML-GSVD is summarized as Algorithm 1.

B. PERFORMANCE OF ROEML-GSVD

Before we move to the design of robust beamformers based on the aforementioned tensor decomposition, let us emphasize the distinction between the CSI-error-robust ROEML-GSVD here proposed and previous contributions, including our earlier OEML-GSVD algorithm offered in [5], and the ML-GSVD scheme of [15], [16].

First notice that due the CSI error-aware channel estimate model of (2), the decomposition error matrices $\boldsymbol{W}_k$ given in (11) contain a new term dependent on the channel estimation error factor γ. As a consequence of the latter, the optimized matrices $\boldsymbol{B}_k$ obtained as in (12) are also functions of the channel estimation error factor γ, thus differing from those obtained under the SotA methods [5], [15]. And naturally, since the other terms $\boldsymbol{C}_k$ and $\boldsymbol{A}$ are computed directly from $\boldsymbol{B}_k$ as per (13) to (16), the decomposition matrices $(\boldsymbol{B}_k,\boldsymbol{C}_k,\boldsymbol{A})$ obtained under the proposed ROEML-GSVD scheme are distinct from those obtained via the ML-GSVD and our earlier OEML-GSVD.

Due to the only slight change in the aforementioned equations, one would be forgiven for considering at a first glance that the distinction between the proposed method and the SotA alternatives is not significant. Such a perception is, however, quite incorrect. Instead, the seemingly small distinction between the ROEML-GSVD solution and previous results in very significant improvement in terms of the accuracy of the decomposition. To see that, let us define the average normalized aggregate decomposition and CSI error at each iteration $\bar{E}_{\mathcal{H}}^{(i)}$, which measures the distance between the true channel tensor $\mathcal{H}$ and its decomposition at the i-th iteration, averaged over multiple channel realizations,

$$\bar{E}_{\mathcal{H}}^{(i)}\triangleq\mathbb{E}\left[\frac{\sum_{k\in\mathcal{K}}\|\boldsymbol{H}_k-\boldsymbol{B}_k^{(i)}\mathbf{C}_k^{(i)}\boldsymbol{A}^{(i)}\|_{\mathrm{F}}^2}{\sum_{k\in\mathcal{K}}\|\boldsymbol{H}_k\|_{\mathrm{F}}^2}\right].\tag{17}$$

By computing $\bar{E}_{\mathcal{H}}^{(i)}$ using the matrices $(\boldsymbol{B}_k,\boldsymbol{C}_k,\boldsymbol{A})$ obtained via each of the distinct methods, and comparing its evolution over the iterations of each technique, we can effectively assess both the accuracies and convergence properties of the different approaches, which is offered in Fig. 3, with simulation parameters following related literature [3], [31], [32], [33] and as summarized in Table 1.

For the sake of providing a lower-bounding reference, it is useful to define the average normalized CSI error, *i.e.*

$$\bar{\delta}_{\mathcal{H}}^2\triangleq\frac{\sum_{k\in\mathcal{K}}\|\boldsymbol{H}_k-\hat{\boldsymbol{H}}_k\|_{\mathrm{F}}^2}{\sum_{k\in\mathcal{K}}\|\boldsymbol{H}_k\|_{\mathrm{F}}^2}.\tag{18}$$

Consider then the results of Fig. 3, which compares curves of the aggregate decomposition and CSI error $\bar{E}_{\mathcal{H}}^{(i)}$ corresponding to the OEML-GSVD of [5], the ML-GSVD of [15], [16], and the here-proposed ROEML-GSVD of Section III-A, for two distinct scenarios with smaller and larger CSI errors. It

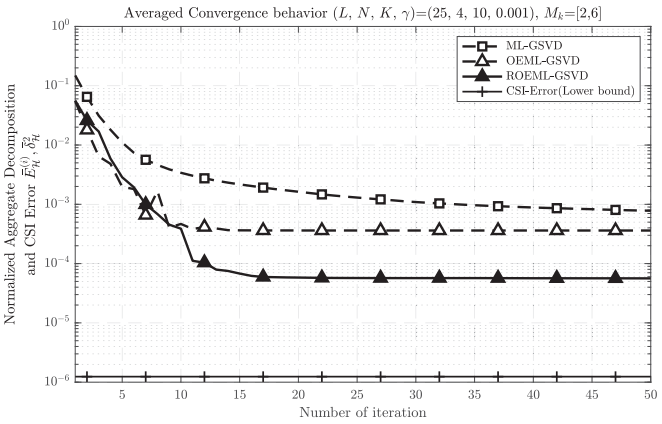

(a) Small CSI Error

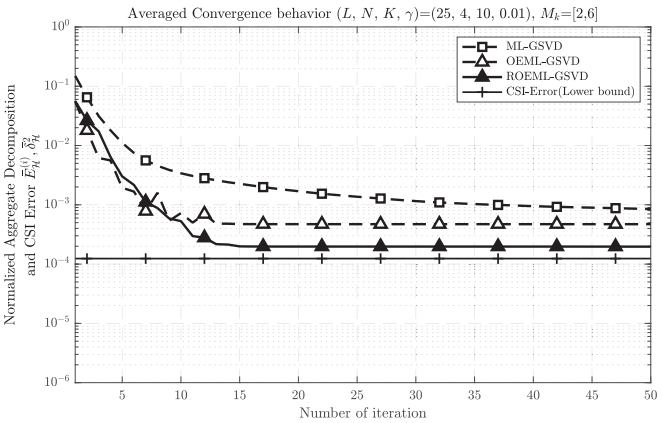

(b) Large CSI Error

FIGURE 3. Convergence of tensor decomposition schemes.

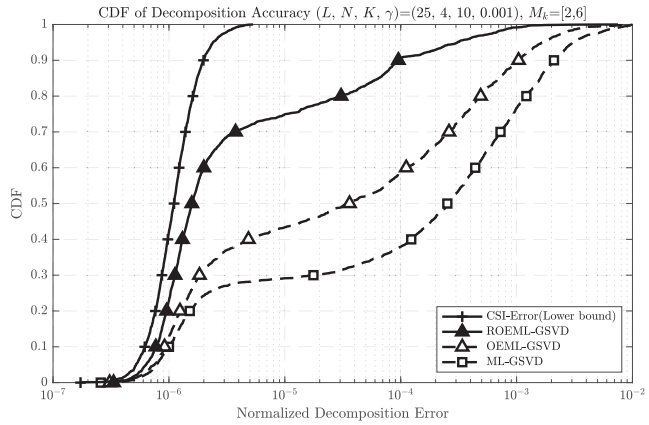

(a) Small CSI Error

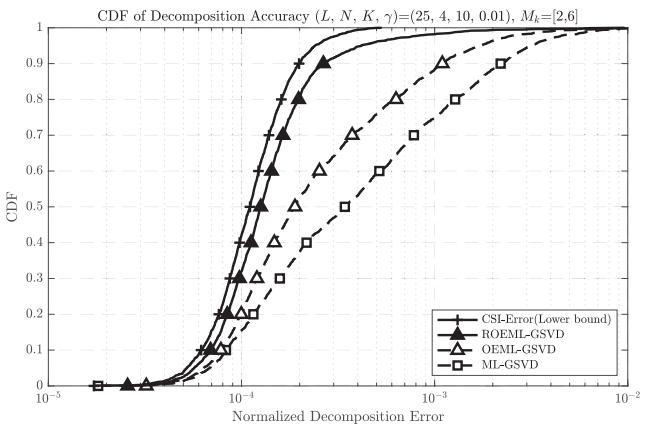

(b) Large CSI Error

FIGURE 4. Statistical accuracy of tensor decomposition schemes.

TABLE 1. Simulation Parameters Used in Figs. 3, 4, 8 and 9

Symbol	Meaning	Value
L	Number of APs	25
N	Number of AP's antenna	4
K	Number of UEs	10
M_k	Number of k-th UE's antenna	[2,6]
γ	CSI error factor	0.01, 0.001
h	Height of antennas	10[m] [3]
f_c	Carrier frequency	2[GHz] [3]
B	Bandwidth	20 [MHz] [3]
D	Length of a side of the square	300[m] [31]
σ^2	Receiver noise variance	-96[dBm] [3]
P^{d}	Downlink TX power constraint	45[dBm]
P_k^{u}	Uplink TX power constraint	20[dBm]

can be seen that indeed the new algorithm has a convergence[3] slope similar to that of the OEML-GSVD.

It is also seen, however, that the ROEML-GSVD continues reducing the decomposition error further, achieving a significantly lower point than the SotA alternatives. The conclusions drawn from Fig. 3 are corroborated by the results of Fig. 4, also with parameters as in Table 1, which shows cumulative distribution functions (CDFs) of $\bar{E}_{\mathcal{H}}^{(i)}$, again compared to the CDF of $\bar{\delta}_{\mathcal{H}}^2$ as a lower-bound.

It is seen, again, that the proposed ROEML-GSVD significantly outperforms SotA schemes, achieving an error distribution much closer to that of the CSI error itself. Another counter-intuitive but quite visible effect that can be seen in Figs. 3 and 4 is that the ROEML-GSVD algorithm performs particularly well in cases under large CSI errors, in which case the proposed method approaches very closely the lower-bounding CSI error level. In other words, under large CSI errors, the new ROEML-GSVD decomposition is almost free of decomposition error, with the average normalized distance between the decomposed matrices $\boldsymbol{B}_k \cdot \boldsymbol{C}_k \cdot \boldsymbol{A}$ and the true channels $\boldsymbol{H}_k$ approaching the CSI error itself.

A fair question at this point is why the ROEML-GSVD algorithm offers such significant reduction in the decomposition error when subject to larger CSI errors, given that these two sources of error are, in principle, independent of one another?

[3]The fact that generalized singular value decomposition (GSVD) methods have good convergence properties is well-known [34], [35], and in the case of the variation here presented, convergence is ensured by preceding work on the convergence of direct fitting approaches [28] and of adaptively iterative thresholding algorithms [30], in addition to the various small quantities δ, ξ, ω and ε utilized to avoid vanishing denominators and ill-conditions.

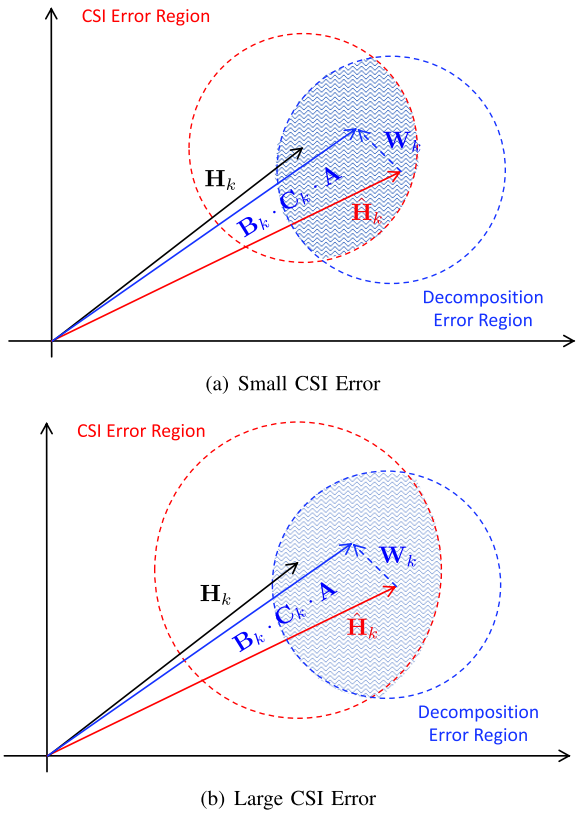

FIGURE 5. Illustration of CSI error-aware decomposition gain.

An intuitive explanation of the phenomenon is as depicted in Fig. 5, which depicts the overlap between the independent CSI error and decomposition error regions.

The figure illustrates how an overlap between the decomposition and CSI error regions actually increases the likelihood that a decomposition in the form $\boldsymbol{B}_k \cdot \boldsymbol{C}_k \cdot \boldsymbol{A}$ obtained around an estimate $\hat{\boldsymbol{H}}_k$, has a shorter distance to the true channel $\boldsymbol{H}_k$, with such a likelihood increasing with the size of the CSI error region.

IV. APPLICATION: TX AND RX BEAMFORMING DESIGN FOR HETEROGENEOUS CF-MMIMO UL AND DL TRANSMISSIONS

A practical application of the ROEML-GSVD technique proposed above is the design of joint TX and RX beamformers for the UL and DL of CF-mMIMO with heterogeneous users, as illustrated in Fig. 6.

A. DOWNLINK BEAMFORMING DESIGN

At the TX side, each BF matrix $\boldsymbol{V}_k^{\mathrm{d}}$ is designed as the right hand side diagonalizer of the common matrix $\boldsymbol{A}^{\mathrm{T}}$, but confined to the select Q_k subspace dimensions. Mathematically we therefore have,

$$\boldsymbol{V}_k^{\mathrm{d}} = \sqrt{\frac{P^{\mathrm{d}}}{\sum_{k' \in \mathcal{K}} Q_{k'}}} \frac{\left(\boldsymbol{A}^{\mathrm{T}}\right)^{\dagger} \mathbf{J}_k}{\| \left(\boldsymbol{A}^{\mathrm{T}}\right)^{\dagger} \mathbf{J}_k \|_{\mathrm{F}}}, \tag{19}$$

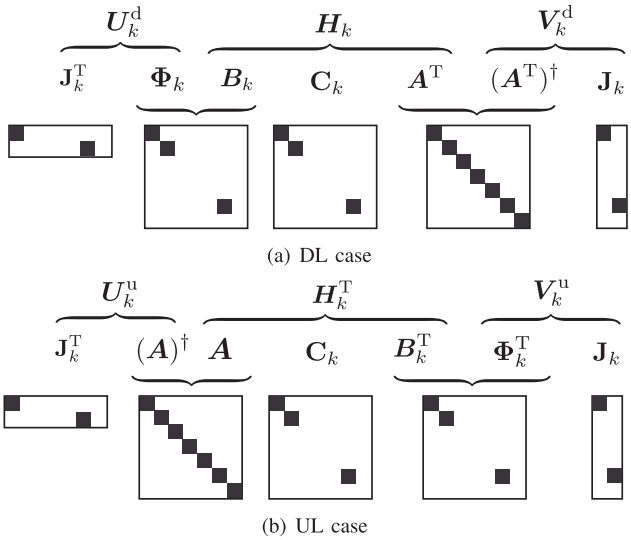

FIGURE 6. Illustration of the proposed beamforming design. Notice that the UL-TX BF is designed with basis on the matrix Φ_k, given in (22a).

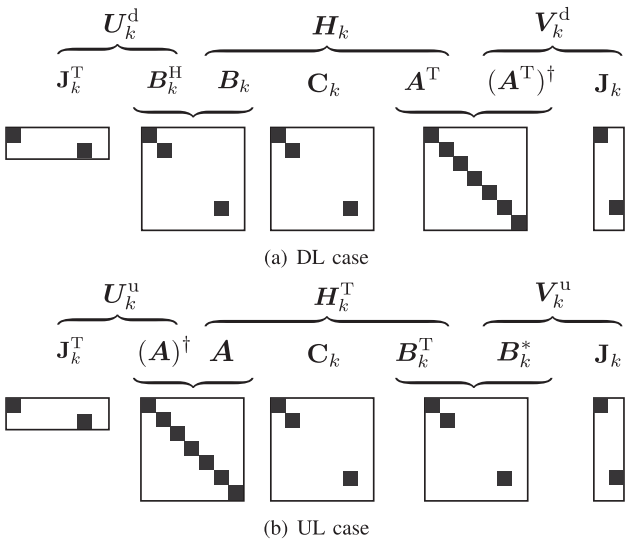

FIGURE 7. Illustration of beamforming designs based on SotA tensor decompositions. Notice that the UL-TX BF is designed based on the conjugate of the solution B_k of the corresponding fitting problems [5], [15].

where P^{d} and $(\cdot)^{\dagger}$ denote the total TX power in DL and the capped pseudo-inverse operation, while $\mathbf{J}_k \in \{0, 1\}^{LN \times Q_k}$ is the subspace selection matrix for the k-th UE, respectively.

In turn, at the RX side, the strategy is to complete, from left hand side, the diagonalization the of the precoded channel matrix, while incorporating robustness to CSI imperfection and decomposition errors, under statistical knowledge of both. To that end, we must therefore design of compensation matrix $\boldsymbol{\Phi}_k \in \mathbb{C}^{LN \times M_k}$ satisfying $\boldsymbol{\Phi}_k \boldsymbol{H}_k \to \boldsymbol{\Gamma}_k$, which can be obtained by solving the following problem

$$\boldsymbol{\Phi}_k = \underset{\boldsymbol{\Phi}_k}{\operatorname{argmin}} \quad \mathbb{E}\left[\| \boldsymbol{\Gamma}_k - \boldsymbol{\Phi}_k \boldsymbol{H}_k \|_{\mathrm{F}}^2 \right], \tag{20}$$

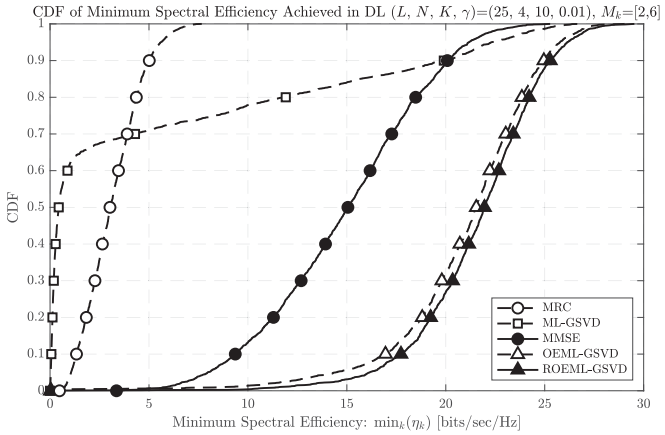

(a) Minimum SE

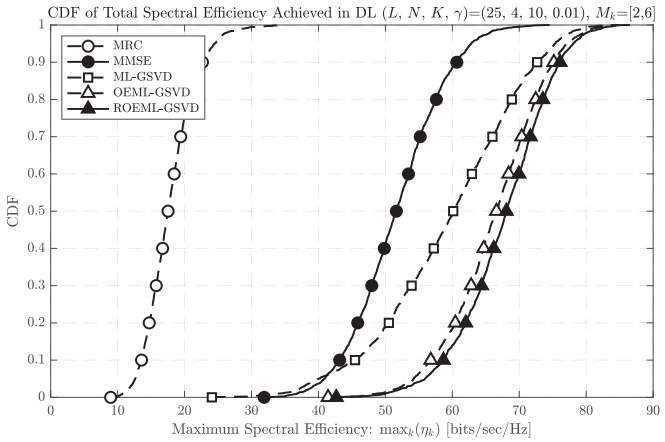

(b) Maximum SE

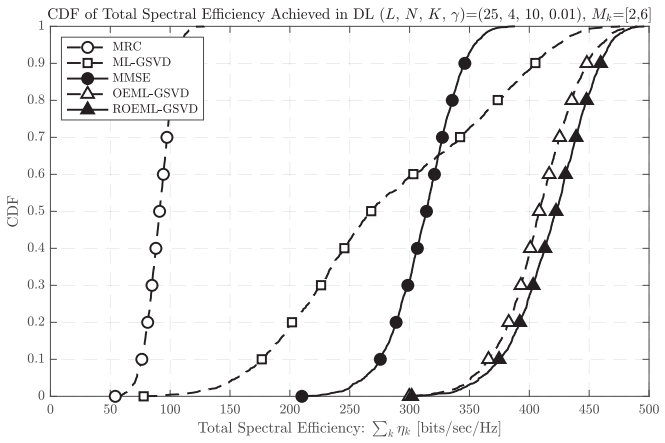

(c) Total SE

FIGURE 8. DL SE of CF-mMIMO systems with various BF schemes.

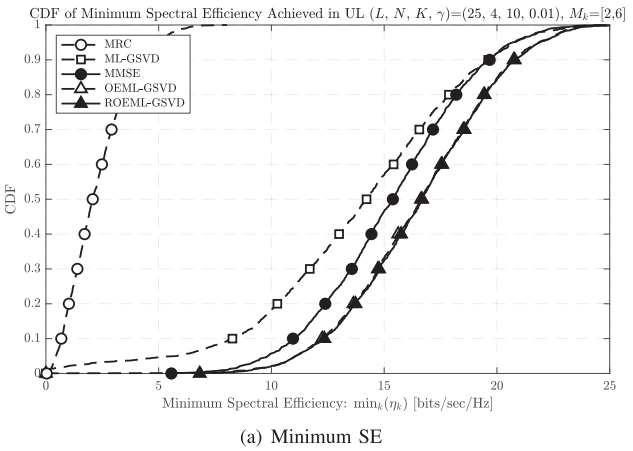

(a) Minimum SE

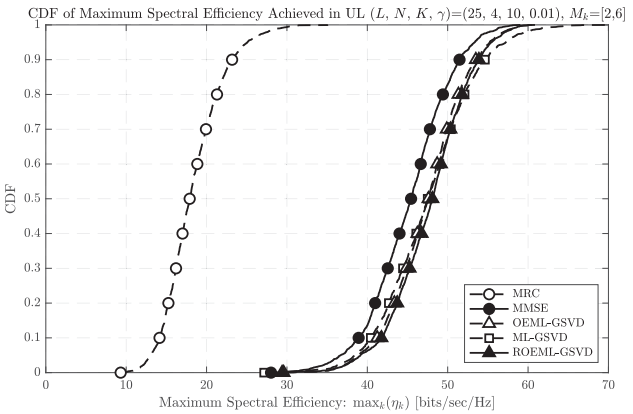

(b) Maximum SE

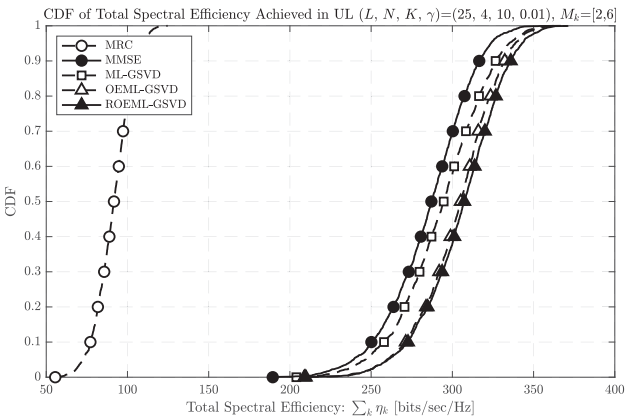

(c) Total SE

FIGURE 9. UL SE of CF-mMIMO systems with various BF schemes.

which readily yields the corresponding Lagrangian

$$\mathcal{L}_{\Phi_k} = \mathbb{E}\left[\left\|\boldsymbol{\Gamma}_k - \boldsymbol{\Phi}_k\left(\boldsymbol{B}_k\boldsymbol{\Gamma}_k + \boldsymbol{W}_k\right)\right\|_{\mathrm{F}}^2\right], \tag{21}$$

such that the Wirtinger solution of (20) is given by

$$\boldsymbol{\Phi}_k = \boldsymbol{\Gamma}_k\boldsymbol{\Gamma}_k^{\mathrm{H}}\boldsymbol{B}_k^{\mathrm{H}}\left(\boldsymbol{B}_k\boldsymbol{\Gamma}_k\boldsymbol{\Gamma}_k^{\mathrm{H}}\boldsymbol{B}_k^{\mathrm{H}} + \mathbb{E}\left[\boldsymbol{W}_k\boldsymbol{W}_k^{\mathrm{H}}\right]\right)^{-1}, \tag{22a}$$

where it can be shown that

$$\mathbb{E}\left[\boldsymbol{W}_k\boldsymbol{W}_k^{\mathrm{H}}\right] = \boldsymbol{B}_k\boldsymbol{\Gamma}_k\boldsymbol{\Gamma}_k^{\mathrm{H}}\boldsymbol{B}_k^{\mathrm{H}} + \frac{1}{1-\gamma^2}\left(\hat{\boldsymbol{H}}_k\hat{\boldsymbol{H}}_k^{\mathrm{H}} + \gamma^2\mathbb{E}\left[\tilde{\boldsymbol{G}}_k\boldsymbol{\Omega}_k\boldsymbol{\Omega}_k^{\mathrm{H}}\tilde{\boldsymbol{G}}_k^{\mathrm{H}}\right]\right) - \frac{1}{\sqrt{1-\gamma^2}}\left(\hat{\boldsymbol{H}}_k\boldsymbol{\Gamma}_k^{\mathrm{H}}\boldsymbol{B}_k^{\mathrm{H}} + \boldsymbol{B}_k\boldsymbol{\Gamma}_k\hat{\boldsymbol{H}}_k^{\mathrm{H}}\right), \tag{22b}$$

and that

$$\mathbb{E}\left[\tilde{\boldsymbol{G}}_k \boldsymbol{\Omega}_k \boldsymbol{\Omega}_k^{\mathrm{H}} \tilde{\boldsymbol{G}}_k^{\mathrm{H}}\right] = N \sum_{\ell \in \mathcal{L}} \rho_{\ell,k}^2 \, \mathbf{I}_{M_k}. \tag{22c}$$

Then, the RX-BF matrix for the k-th user becomes simply

$$\boldsymbol{U}_k^{\mathrm{d}} = \mathbf{J}_k^{\mathrm{T}} \boldsymbol{\Phi}_k. \tag{23}$$

B. UPLINK BEAMFORMING DESIGN

Under the assumption of channel reciprocity, the channel matrix in UL model is just the transpose of the DL channel matrix, such that the UL-BF design is also just as transpose of its DL-BF counterpart, except for normalization and scaling. Therefore, in contrast to the DL, at the TX side each BF matrix $\boldsymbol{V}_k^{\mathrm{u}}$ is designed as the right hand side diagonalizer of the matrix $\boldsymbol{H}_k^{\mathrm{T}}$, *i.e.*,

$$\boldsymbol{V}_k^{\mathrm{u}} = \sqrt{P_k^{\mathrm{u}}} \frac{\boldsymbol{\Phi}_k^{\mathrm{T}} \mathbf{J}_k}{\|\boldsymbol{\Phi}_k^{\mathrm{T}} \mathbf{J}_k\|_{\mathrm{F}}}, \tag{24}$$

where P_k^{u} denotes the TX power of k-th UE in UL.

In turn, at the RX side, the beamformer amounts to the left hand side diagonalizer of the precoded channel matrix $\boldsymbol{H}_k^{\mathrm{T}}$, such that the RX-BF matrix for the k-th user becomes

$$\boldsymbol{U}_k^{\mathrm{u}} = \mathbf{J}_k^{\mathrm{T}} (\boldsymbol{A})^{\dagger}. \tag{25}$$

C. QUALITATIVE COMPARISON WITH SOTA ALTERNATIVES

Before we continue with an assessment of the improvement achieved by the aforementioned beamformers compared to SotA methods, let us first address the qualitative differences between the proposed technique and SotA alternatives. For consistency, the same notation used above for the DL-TX, DL-RX, UL-TX and UL-RX beamformers, namely, $\boldsymbol{V}_k^{\mathrm{d}}$, $\boldsymbol{U}_k^{\mathrm{d}}$, $\boldsymbol{V}_k^{\mathrm{u}}$ and $\boldsymbol{U}_k^{\mathrm{u}}$ will be used for the SotA methods.

The maximum ratio combiner (MRC) BFs are given by [1]

$$\boldsymbol{V}_{k:\mathrm{MRC}}^{\mathrm{d}} = \sqrt{\frac{P^{\mathrm{d}}}{\sum_{k' \in \mathcal{K}} Q_{k'}}} \frac{\boldsymbol{H}_k^{\mathrm{H}}}{\|\boldsymbol{H}_k^{\mathrm{H}}\|_{\mathrm{F}}} \quad \text{and} \quad \boldsymbol{U}_{k:\mathrm{MRC}}^{\mathrm{d}} = \mathbf{I}_{M_k}, \tag{26a}$$

$$\boldsymbol{V}_{k:\mathrm{MRC}}^{\mathrm{u}} = \sqrt{P_k^{\mathrm{u}}} \cdot \mathbf{I}_{M_k} \quad \text{and} \quad \boldsymbol{U}_{k:\mathrm{MRC}}^{\mathrm{u}} = \boldsymbol{H}_k^{*}. \tag{26b}$$

Comparing the DL-TX beamforming matrix $\boldsymbol{V}_k^{\mathrm{d}}$ of (19) against $\boldsymbol{V}_{k:\mathrm{MRC}}^{\mathrm{d}}$ of (26a), as well as the UL-RX beamforming matrix $\boldsymbol{U}_k^{\mathrm{u}}$ of (25) against $\boldsymbol{U}_{k:\mathrm{MRC}}^{\mathrm{u}}$ of (26b), it is visible how the MRC design does not account for the interference among the various K users, since the transmit beamformers $\boldsymbol{V}_{k:\mathrm{MRC}}^{\mathrm{d}}$ and $\boldsymbol{V}_{k':\mathrm{MRC}}^{\mathrm{d}}$ (or correspondingly $\boldsymbol{U}_{k:\mathrm{MRC}}^{\mathrm{u}}$ and $\boldsymbol{U}_{k':\mathrm{MRC}}^{\mathrm{u}}$), with $k \neq k'$ are designed independently, such that the system is at the mercy of the distance between the channels $\boldsymbol{H}_k$ and $\boldsymbol{H}_\ell$ to spatially separate users.

That limitation is partially eleviated by the minimum mean square error (MMSE) design, whose BFs are given by [3]

$$\boldsymbol{V}_{k:\mathrm{MMSE}}^{\mathrm{d}} = \sqrt{\frac{P^{\mathrm{d}}}{\sum_{k' \in \mathcal{K}} Q_{k'}}} \frac{\left(\sum_{k'} \boldsymbol{H}_{k'}^{\mathrm{H}} \boldsymbol{H}_{k'} + \sigma_k^2 \mathbf{I}_{LN}\right)^{-1} \boldsymbol{H}_k^{\mathrm{H}}}{\| \left(\sum_{k'} \boldsymbol{H}_{k'}^{\mathrm{H}} \boldsymbol{H}_{k'} + \sigma_k^2 \mathbf{I}_{LN}\right)^{-1} \boldsymbol{H}_k^{\mathrm{H}} \|_{\mathrm{F}}}, \tag{27a}$$

$$\boldsymbol{U}_{k:\mathrm{MMSE}}^{\mathrm{d}} = \mathbf{I}_{M_k}, \tag{27b}$$

$$\boldsymbol{V}_{k:\mathrm{MMSE}}^{\mathrm{u}} = \sqrt{P_k^{\mathrm{u}}} \cdot \mathbf{I}_{M_k} \tag{27c}$$

$$\boldsymbol{U}_{k:\mathrm{MMSE}}^{\mathrm{u}} = \boldsymbol{H}_k^{*} \left(\sum_{k'} \boldsymbol{H}_{k'}^{\mathrm{T}} \boldsymbol{H}_{k'}^{*} + \sigma_k^2 \mathbf{I}_{LN} \right)^{-1}. \tag{27d}$$

In this case, some reduction of interference among users is accomplished in particular via $\boldsymbol{V}_{k:\mathrm{MMSE}}^{\mathrm{d}}$ and $\boldsymbol{U}_{k:\mathrm{MMSE}}^{\mathrm{u}}$, where the aggregate interference onto a k-th user due to the remaining $K-1$ users is essentially treated as noise and accounted for accordingly. It is evident from the expressions, however, that for a sufficiently large K, the terms $\sum_{k'} \boldsymbol{H}_{k'}^{\mathrm{H}} \boldsymbol{H}_{k'}$ and $\sum_{k'} \boldsymbol{H}_{k'}^{\mathrm{T}} \boldsymbol{H}_{k'}^{*}$ tend to Gaussian random matrices, rendering the approach ineffective in such scenarios.

In contrast to such approaches, the BF designs obtained from SotA tensor decompositions, namely, the ML-GSVD and the OEML-GSVD, are given by [5]

$$\boldsymbol{V}_{k:\mathrm{SotA\text{-}TD}}^{\mathrm{d}} = \sqrt{\frac{P^{\mathrm{d}}}{\sum_{k' \in \mathcal{K}} Q_{k'}}} \frac{\left(\boldsymbol{A}_{\mathrm{SotA\text{-}TD}}^{\mathrm{T}}\right)^{\dagger} \mathbf{J}_{k:\mathrm{SotA\text{-}TD}}}{\| \left(\boldsymbol{A}_{\mathrm{SotA\text{-}TD}}^{\mathrm{T}}\right)^{\dagger} \mathbf{J}_{k:\mathrm{SotA\text{-}TD}} \|_{\mathrm{F}}}, \tag{28a}$$

$$\boldsymbol{U}_{k:\mathrm{SotA\text{-}TD}}^{\mathrm{d}} = \mathbf{J}_{k:\mathrm{SotA\text{-}TD}}^{\mathrm{T}} \boldsymbol{B}_{k:\mathrm{SotA\text{-}TD}}^{\mathrm{H}} \tag{28b}$$

$$\boldsymbol{V}_{k:\mathrm{SotA\text{-}TD}}^{\mathrm{u}} = \sqrt{P_k^{\mathrm{u}}} \frac{\boldsymbol{B}_{k:\mathrm{SotA\text{-}TD}}^{*} \mathbf{J}_{k:\mathrm{SotA\text{-}TD}}}{\| \boldsymbol{B}_{k:\mathrm{SotA\text{-}TD}}^{*} \mathbf{J}_{k:\mathrm{SotA\text{-}TD}} \|_{\mathrm{F}}}, \tag{28c}$$

$$\boldsymbol{U}_{k:\mathrm{SotA}}^{\mathrm{u}} = \mathbf{J}_{k:\mathrm{SotA\text{-}TD}}^{\mathrm{T}} (\boldsymbol{A}_{\mathrm{SotA\text{-}TD}})^{\dagger}. \tag{28d}$$

Referring to Fig. 7, and comparing (27a) to (27d) against (28a) to (28d), it is clear how the BF strategy based on tensor decomposition offers further improvement over the MMSE, by making all beamforming matrices for a given k-th consistently designed with basis on the matrix $\boldsymbol{J}_k$, which essentially extracts from the corresponding decomposed slice $\boldsymbol{H}_k = \boldsymbol{B}_k \cdot \boldsymbol{C}_k \cdot \boldsymbol{A}$ of the channel tensor $\boldsymbol{\mathcal{H}}$, the best private subspace of the k-th user. In other words, in contrast to MMSE, the tensor proposed approach handles multiuser interference not in an aggregate manner, but rather in an optimized fashion, under a given criterion.

In light of the above, there are two distinct ways in which the technique here proposed improves over the SotA on DL/UL-TX/RX joint beamforming for CF-mMIMO systems with heterogeneous users and imperfect CSI. The first is in offering a more accurate decomposition itself, by reducing the decomposition error compared to those of the ML-GSVD of [15], [16] and the OEML-GSVD of [5], as already demonstrated in Section III-B And the second is in improving the BF

design, by introducing the compensation matrix $\boldsymbol{\Phi}_k$, computed with basis on the criterion described by (20), and which seeks to mitigate, in an MMSE sense, the impact of any channel estimation and/or decomposition errors still remaining, as visible from its closed form expression given in (22a). This latter distinction is explicit in the differences between the DL-RX beamformers $\boldsymbol{U}_k^{\mathrm{d}}$ and $\boldsymbol{U}_{k:\mathrm{SotA\text{-}TD}}^{\mathrm{d}}$ of (23) and (28b), respectively, and between the UL-TX beamformers $\boldsymbol{V}_k^{\mathrm{u}}$ and $\boldsymbol{V}_{k:\mathrm{SotA\text{-}TD}}^{\mathrm{u}}$ of (24) and (28c), respectively.

Regarding complexity, since the proposed ROEML-GSVD is a modification of OEML-GSVD, the computational cost of BF schemes based on both methods is the same, which was shown in [5] to be of the order

$$\mathcal{O}\left(i_{\max}K(LN)^3 + i_{\max}(LN)^2\left(K + \sum\nolimits_{k=1}^{K} M_k\right)\right), \tag{29}$$

thus similar to that of the classic MMSE beamformer, namely

$$\mathcal{O}\left((LN)^3 + (LN)^2(K+1)\sum\nolimits_{k=1}^{K} M_k\right), \tag{30}$$

which is a rather remarkable feature of the proposed method, given its substantial performance gains.

V. NUMERICAL RESULTS

Let us finally demonstrate the efficacy of the application of the proposed ROEML-GSVD tensor decomposition to the beamforming problem in CF-mMIMO systems with heterogeneous users and imperfect CSI acquisition.

To that end, we compare the CDFs of the minimum, maximum and total DL and UL SEs (*i.e.* rates in bits/sec/Hz) achieved by the system using each of the BF schemes considered, with simulation parameters as given in Table 1.

The results, which follow a format typical of CF-mMIMO literature [3], [31], [32], [33] are shown in Figs. 8 and 9, and indicate that the proposed ROEML-GSVD-based BF design outperforms the MRC, MMSE and ML-GSVD SotA alternatives in all cases, with the gains most relevant in the DL mode. The results also show that the improvement in SE is particularly similar for the lowest rate and highest rate users, indicating that the proposed method offers a degree of enhancement in terms of fairness as well, although we omit plots on that figure of merit due lack of space.

VI. CONCLUSION

We proposed a new robust tensor decomposition algorithm with application to the design of joint TX and RX BF at both the DL and the UL of CF-mMIMO systems.

In particular, the new decomposition, dubbed the ROEML-GSVD, is designed to minimize the degradation in the DL and UL BF design due to both the tensor decomposition error and the CSI imperfection. Numerical results demonstrate that despite a computational complexity similar to that of MMSE beamformers, the proposed ROEML-GSVD-based BF method leads to significant increases in the data rate achieved by CF-mMIMO systems serving heterogeneous users with distinct numbers of antennas.

REFERENCES

[1] H. Q. Ngo, A. Ashikhmin, H. Yang, E. G. Larsson, and T. L. Marzetta, "Cell-free massive MIMO versus small cells," *IEEE Trans. Wireless Commun.*, vol. 16, no. 3, pp. 1834–1850, Mar. 2017.

[2] E. Björnson and L. Sanguinetti, "Scalable cell-free massive MIMO systems," *IEEE Trans. Commun.*, vol. 68, no. 7, pp. 4247–4261, Jul. 2020.

[3] E. Björnson and L. Sanguinetti, "Making cell-free massive MIMO competitive with MMSE processing and centralized implementation," *IEEE Trans. Wireless Commun.*, vol. 19, no. 1, pp. 77–90, Jan. 2020.

[4] S. Buzzi and C. D'Andrea, "Cell-free massive MIMO: User-centric approach," *IEEE Wireless Commun. Lett.*, vol. 6, no. 6, pp. 706–709, Dec. 2017.

[5] K. Ando, H. Iimori, G. T. F. de Abreu, and K. Ishibashi, "User-heterogeneous cell-free massive MIMO downlink and uplink beamforming via tensor decomposition," *IEEE Open J. Commun. Soc.*, vol. 3, pp. 740–758, 2022.

[6] X. Zhang, H. Qi, X. Zhang, and L. Han, "Energy-efficient resource allocation and data transmission of cell-free Internet of Things," *IEEE Internet Things J.*, vol. 8, no. 20, pp. 15107–15116, Oct. 2021.

[7] A. A. Polegre, L. Sanguinetti, and A. G. Armada, "Pilot decontamination processing in cell-free massive MIMO," *IEEE Commun. Lett.*, vol. 25, no. 12, pp. 3990–3994, Dec. 2021.

[8] T. C. Mai, H. Q. Ngo, and T. Q. Duong, "Downlink spectral efficiency of cell-free massive MIMO systems with multi-antenna users," *IEEE Trans. Commun.*, vol. 68, no. 8, pp. 4803–4815, Aug. 2020.

[9] X. Li, J. Zhang, Z. Wang, B. Ai, and D. W. K. Ng, "Cell-free massive MIMO with multi-antenna users over Weichselberger Rician channels," *IEEE Trans. Veh. Technol.*, vol. 71, no. 11, pp. 12368–12373, Nov. 2022.

[10] K. Shen, W. Yu, L. Zhao, and D. P. Palomar, "Optimization of MIMO device-to-device networks via matrix fractional programming: A minorization–maximization approach," *IEEE/ACM Trans. Netw.*, vol. 27, no. 5, pp. 2164–2177, Oct. 2019.

[11] S. Buzzi, C. D'Andrea, M. Fresia, Y.-P. Zhang, and S. Feng, "Pilot assignment in cell-free massive MIMO based on the hungarian algorithm," *IEEE Wireless Commun. Lett.*, vol. 10, no. 1, pp. 34–37, Jan. 2021.

[12] T. C. Mai, H. Q. Ngo, M. Egan, and T. Q. Duong, "Pilot power control for cell-free massive MIMO," *IEEE Trans. Veh. Technol.*, vol. 67, no. 11, pp. 11264–11268, Nov. 2018.

[13] T. Yoo and A. Goldsmith, "Capacity and power allocation for fading MIMO channels with channel estimation error," *IEEE Trans. Inf. Theory*, vol. 52, no. 5, pp. 2203–2214, May 2006.

[14] A. J. Goldsmith and P. P. Varaiya, "Capacity of fading channels with channel side information," *IEEE Trans. Inf. Theory*, vol. 43, no. 6, pp. 1986–1992, Nov. 1997.

[15] L. Khamidullina, A. L. F. de Almeida, and M. Haardt, "Multilinear generalized singular value decomposition (ML-GSVD) with application to coordinated beamforming in multi-user MIMO systems," in *Proc. IEEE Int. Conf. Acoust. Speech Signal Process.*, Barcelona, Spain, 2020, pp. 4587–4591.

[16] L. Khamidullina, A. L. F. de Almeida, and M. Haardt, "Multilinear generalized singular value decomposition (ML-GSVD) and its application to multiuser MIMO systems," *IEEE Trans. Signal Process.*, vol. 70, pp. 2783–2797, 2022.

[17] D. Jaramillo-Ramírez, M. Kountouris, and E. Hardouin, "Coordinated multi-point transmission with imperfect CSI and other-cell interference," *IEEE Trans. Wireless Commun.*, vol. 14, no. 4, pp. 1882–1896, Apr. 2015.

[18] L. Du, L. Li, P. Zhang, D. Miao, and Z. Liu, "Vector perturbation precoding under imperfect CSI and inaccurate power scaling factors," *IEEE Access*, vol. 7, pp. 89162–89171, 2019.

[19] Y. Xiong, S. Sun, L. Qin, N. Wei, L. Liu, and Z. Zhang, "Performance analysis on cell-free massive MIMO with capacity-constrained fronthauls and variable-resolution ADCs," *IEEE Syst. J.*, vol. 16, no. 2, pp. 3296–3307, Jun. 2022.

[20] H. Bolcskei, M. Borgmann, and A. J. Paulraj, "Impact of the propagation environment on the performance of space-frequency coded MIMO-OFDM," *IEEE J. Sel. Areas Commun.*, vol. 21, no. 3, pp. 427–439, Apr. 2003.
[21] 3GPP, "Further advancements for E-UTRA physical layer aspects (release 9)," 3GPP, Tech. Rep. TR 36.913, Mar. 2017.
[22] C. Wang and R. D. Murch, "Adaptive downlink multi-user MIMO wireless systems for correlated channels with imperfect CSI," *IEEE Trans. Wireless Commun.*, vol. 5, no. 9, pp. 2435–2446, Sep. 2006.
[23] M. Dai, B. Clerckx, D. Gesbert, and G. Caire, "A rate splitting strategy for massive MIMO with imperfect CSIT," *IEEE Trans. Wireless Commun.*, vol. 15, no. 7, pp. 4611–4624, Jul. 2016.
[24] A. Lapidoth and P. Narayan, "Reliable communication under channel uncertainty," *IEEE Trans. Inf. Theory*, vol. 44, no. 6, pp. 2148–2177, Oct. 1998.
[25] M. S. Kay, *Fundamentals of Statistical Signal Processing: Estimation Theory*. Upper Saddle River, NJ, USA: Prentice-Hall, 1993.
[26] J. Baltersee, G. Fock, and H. Meyr, "Achievable rate of MIMO channels with data-aided channel estimation and perfect interleaving," *IEEE J. Sel. Areas Commun.*, vol. 19, no. 12, pp. 2358–2368, Dec. 2001.
[27] B. Hassibi and B. M. Hochwald, "How much training is needed in multiple-antenna wireless links?," *IEEE Trans. Inf. Theory*, vol. 49, no. 4, pp. 951–963, Apr. 2003.
[28] H. Kiers, J. Berge, and R. Bro, "PARAFAC2—Part I. A direct fitting algorithm for the PARAFAC2 model," *J. Chemometrics*, vol. 13, pp. 275–294, May 1999.
[29] P. Comon, "Tensors : A brief introduction," *IEEE Signal Process. Mag.*, vol. 31, no. 3, pp. 44–53, 2014.
[30] Y. Wang, J. Zeng, Z. Peng, X. Chang, and Z. Xu, "Linear convergence of adaptively iterative thresholding algorithms for compressed sensing," *IEEE Trans. Signal Process.*, vol. 63, no. 11, pp. 2957–2971, 2015.
[31] F. Tan, P. Wu, Y.-C. Wu, and M. Xia, "Energy-efficient non-orthogonal multicast and unicast transmission of cell-free massive MIMO systems with SWIPT," *IEEE J. Sel. Areas Commun.*, vol. 39, no. 4, pp. 949–968, 2021.
[32] J. Qiu, K. Xu, X. Xia, Z. Shen, and W. Xie, "Downlink power optimization for cell-free massive MIMO over spatially correlated Rayleigh fading channels," *IEEE Access*, vol. 8, pp. 56214–56227, 2020.
[33] S. Chen, J. Zhang, E. Björnson, J. Zhang, and B. Ai, "Structured massive access for scalable cell-free massive MIMO systems," *IEEE J. Sel. Areas Commun.*, vol. 39, no. 4, pp. 1086–1100, Apr. 2021.
[34] Y. Guan, M. T. Chu, and D. Chu, "Convergence analysis of an SVD-based algorithm for the best rank-1 tensor approximation," *Linear Algebra Appl.*, vol. 555, pp. 53–69, 2018.
[35] A. Buccini, M. Pasha, and L. Reichel, "Generalized singular value decomposition with iterated Tikhonov regularization," *J. Comput. Appl. Math.*, vol. 373, 2020, Art. no. 112276.